Circulation: Genomic and Precision Medicine

ORIGINAL ARTICLE

Novel Truncating Variant c.1222DupC in *RBM20* Causes Cardiomyopathy Consistent With Haploinsufficiency

Priyanka Pant, PhD; Yong Huang, MD; Zakiya Ghouse, MSc; Fang Bai, PhD; Elena Kemmling, MSc; Laura Konrad; Ahmed Alameldeen, MSc; Rebecca Kistler; Timon Seeger, MD; Michael Gotthardt, MD; Victoria N. Parikh, MD; Maarten M.G. van den Hoogenhof, PhD

BACKGROUND: RBM20 (RNA binding motif protein 20) is a cardiac splicing factor responsible for the splicing of several cardiac genes such as titin (*TTN*), triadin (*TRDN*), ryanodine receptor 2 (*RYR2*), PDZ and LIM domain protein 1 (*PDLIM1*), and calcium/calmodulin-dependent protein kinase II (*CAMK2D*). Pathogenic variants in *RBM20* are a major cause of familial dilated cardiomyopathy, and lead to missplicing of RBM20 target genes.

METHODS: We identified a patient with a novel *RBM20* variant, and expressed the human and mouse-equivalent variant in neonatal rat cardiomyocytes and HEK293 cells. We performed splicing assays, and assessed protein expression and stability. Furthermore, we generated heterozygous *RBM20*-c.1222DupC human induced pluripotent stem cells, differentiated these into human induced pluripotent stem cell-derived cardiomyocytes, and evaluated splicing changes and calcium handling.

RESULTS: We describe a novel heterozygous truncating variant, *RBM20*-c.1222DupC, identified in a patient with mitral valve prolapse and late-onset familial dilated cardiomyopathy. The variant introduces a premature termination codon and generates a truncated protein of ≈55 kDa in vitro. Splicing assays demonstrated complete loss of activity and no dominant-negative effect on wild-type RBM20. The truncated protein localized to both the cytoplasm and nucleus, partially colocalizing with wild-type RBM20, despite lacking the RS and RRM domains. Western blot analysis of endogenous RBM20 in human induced pluripotent stem cell-derived cardiomyocytes carrying the variant revealed a strong reduction in RBM20 protein levels. Reverse transcriptase-polymerase chain reaction revealed splicing defects in canonical RBM20 targets, and RNA sequencing identified widespread splicing abnormalities, including in established RBM20 targets (*TTN*, *RYR2*, *CAMK2D*, and *CACNA1G*). Finally, we observed increased calcium transients.

CONCLUSIONS: Together, these findings establish *RBM20*c.1222DupC as a truncating variant that causes dilated cardiomyopathy likely through haploinsufficiency.

Key Words: animals ■ cytoplasm ■ humans ■ mice ■ rats

Missense variants in *RBM20* are an established cause of dilated cardiomyopathy (DCM) and account for ≈3% to 6% of familial DCM cases.[1] RBM20 (RNA binding motif protein 20) regulates the splicing of multiple cardiac genes, including titin (*TTN*), ryanodine receptor 2 (*RYR2*), LIM domain binding 3 (*LDB3*), and calcium/calmodulin-dependent protein kinase II delta (*CAMK2D*).[1] RBM20 contains several functional regions: a leucine/proline-rich region, 2 zinc finger domains, an RNA recognition motif, an arginine/

Correspondence to: Maarten M.G. van den Hoogenhof, PhD, Institute of Experimental Cardiology, Medical Faculty Heidelberg, Heidelberg University, Eppelheimer Strasse 8, 69115 Heidelberg, Germany. Email maarten.hoogenhof@cardioscience.uni-heidelberg.de

This manuscript was sent to Julie De Backer, MD, PhD, Guest Editor, for review by expert referees, editorial decision, and final disposition.
Supplemental Material is available at https://www.ahajournals.org/doi/suppl/10.1161/CIRCGEN.125.005471.

Circulation: Genomic and Precision Medicine is available at www.ahajournals.org/journal/circgen

Nonstandard Abbreviations and Acronyms

DCM	dilated cardiomyopathy
GWAS	genome-wide association study
hiPSC	human induced pluripotent stem cell
hiPSC-CM	human induced pluripotent stem cell-derived cardiomyocyte
NRCM	neonatal rat cardiomyocyte
PE	prime editing
RBM20	RNA binding motif protein 20
RS	arginine/serine rich
SE	exon skipping
TNPO3	transportin 3
WT	wild-type

serine-rich (RS) domain, and a glutamic acid-rich region. Although variants occur throughout the gene, a hotspot in the RS domain in exon 9 is associated with early-onset and severe disease, frequently with arrhythmia.[1,2] While wild-type (WT) RBM20 typically exhibits a characteristic bipunctate nuclear pattern, RBM20 with RS-domain missense variants mislocalizes to the cytoplasm, where it forms ribonucleoprotein condensates or aggregates. RS-domain variants include p.P633L (c.1898C>T) and p.R634Q (c.1901G>A) or p.R634W (c.1900C>T), which are associated with severe DCM.[3–5] Both P633L and R634Q mislocalize RBM20, while P633L only produces partial mislocalization.[3,6] Additional RS-domain variants, including p.S635A (c.1903T>G), p.R636C (c.1906C>T), and p.P638L (c.1913C>T), also show cytoplasmic mislocalization along with the reported early-onset of the DCM phenotype.[7,8] These variants disrupt the interaction of RBM20 with TNPO3 (transportin 3), its nuclear importer, leading to its mislocalization.[6] Outside the RS domain, variants in the glutamic acid-rich region such as p.E913K (c.2737G>A), p.V914A (c.2741T>C), and p.L908P (c.2723T>C) are associated with DCM without cytoplasmic mislocalization.[7,9,10] Mechanistically, the function of the E-rich domain is not entirely clear, although decreased stability of RBM20-E913K suggests that this region could be essential for maintaining protein stability.[10] The p.I536T (c.1607T>C) variant in the RNA recognition motif domain, which was identified in a patient with sudden cardiac death, impairs splicing in vitro. However, *Rbm20*^{538T} knock-in mice do not exhibit early sudden death, which suggests that loss of splicing alone may be insufficient to reproduce the early and severe human phenotype.[11,12] Recent work indicates that truncating *RBM20* variants are also associated with arrhythmogenic DCM, although on average they show lower penetrance and a milder clinical course than canonical RS-domain missense variants.[13–16] Overall, these data suggest that while pathogenic *RBM20* variants all lead to cardiac disease, RS-domain variants lead to a more severe phenotype.[14] The molecular mechanism(s) underlying RBM20 cardiomyopathy are not entirely clear, but at least 2 partially distinct mechanisms of RBM20-mediated disease have been proposed. The first is the loss-of-function that leads to missplicing of key cardiac genes, which happens with all disease-causing variants. The second is the mislocalization of RBM20 with condensate formation, which seems to be an additional toxic gain-of-function, that occurs with RS-domain variants. Since patients with these variants would have both missplicing of RBM20 targets and mislocalization of RBM20, this aligns with the heightened arrhythmia risk and DCM severity observed in these patients.[17] Here, we report a novel truncating variant in *RBM20*, a duplication (c.1222DupC in exon 2), which leads to a frameshift and premature stop codon, identified in a patient with mitral valve prolapse and regurgitation, who developed persistent DCM after mitral valve repair. In addition, family history included multiple early deaths, suspicious of sudden arrhythmic cause. In functional studies, we show that the truncated protein is less stable, lacks splicing regulatory activity, has no dominant-negative effect, and shows a mixed nuclear and cytoplasmic distribution. These findings are consistent with haploinsufficiency as the disease mechanism for this *RBM20* variant.

METHODS

Clinical data were collected under an institutional review board (Stanford Medicine)-approved waiver of consent.

Data Availability

All data from this study have been made publicly available in the GEO database under accession number GSE308500.

Prime Editing (PE) of hiPSC Line

To introduce the pathogenic P408fs*8 (c.1222DupC) variant into the *RBM20* gene, we used the PE2 prime editor and PE3 nickase system as previously described.[18] pegRNA and PE3 nicking sgRNA were designed using pegFinder (http://pegfinder.sidichenlab.org), and oligo sequences are listed in Table S1. Human induced pluripotent stem cells (hiPSCs) from a healthy individual were electroporated with a 1:1:1 DNA mixture of PE2-GFP, PE2-pegRNA, and PE3-nicking sgRNA using the Neon Transfection System (1100 V, 30 ms, 1 pulse). The following day, GFP-positive cells were sorted via FACS (BD FACSymphony S6) and single-cell cloned into 96-well plates containing CloneR (Stemcell Technologies). Eleven days post-sorting, colonies were picked, genomic DNA was extracted using QuickExtract (Biosearch Technologies), and genotyping was performed using the primers listed in Table S1.

hiPSC Differentiation

Differentiation toward cardiomyocytes was performed following a small molecule Wnt activation/inhibition protocol. Media was changed to RPMI-B27 without insulin (Life Technologies)

supplemented with 4 to 6 µM CHIR99021 (TargetMol). Seventy-two hours later, medium was switched to RPMI-B27 without insulin supplemented with 3 µM IWP (Selleck Chemicals). After 48 hours, the medium was switched to RPMI supplemented with B27 with chemically defined media minus insulin for 2 days, then replaced by RPMI-B27 with insulin (Life Technologies) and refreshed every 2 days. Beating human induced pluripotent stem cell-derived cardiomyocytes (hiPSC-CMs) were observed from day 8 to 10 post-differentiation. On day 13 post-differentiation, cells were transiently cultured in RPMI without D-glucose (Life Technologies) and with B27 minus insulin and supplemented with 0.2% lactate (Sigma) for 96 hours for metabolic selection of iPSC-CM populations. Fully differentiated iPSC-CMs were maintained in RPMI medium supplemented with B27. All experiments were conducted with iPSC-CMs between 35 and 45 days after differentiation.

Calcium Transient Measurement in hiPSC-CMs

For ratiometric calcium imaging, dissociated hiPSC-CMs were seeded on Matrigel-coated 35 mm Glass bottom dish (220.110.022, thickness 1.5 mm, IBL). After 4 days, cells were loaded with 2 µM Fura-2 AM (Thermo Fisher Scientific, F1221) with 0.02% Pluronic F-127 (Thermo Fisher Scientific, P3000MP) in Tyrode's solution for 30 min at 37 °C temperature, followed by washing with Tyrode solution. iPSC-CMs were field-stimulated at 0.5 Hz at 37 °C. Single-cell Ca^{2+} imaging was conducted on a Axio Observer 7 microscope with 40× oil immersion objective. Fura-2 was excited at 340 nm and 380 nm wavelength using a Lambda DG-4 ultra-high-speed wavelength switcher (Sutter Instrument), and the emission of Fura-2 was collected over 510 nm wavelength. Raw data exported from Zeiss Axio Observer were analyzed using a custom Python script (https://github.com/GeorgeMcMullen/CalciPy) built specifically to automate processing of ratiometric calcium imaging data.

Isolation of Neonatal Rat Cardiomyocytes (NRCMs)

One- to two-day-old Wistar rat pups were used for the isolation of ventricular cardiomyocytes using the Neonatal Heart Dissociation Kit (130-098-373, Miltenyi Biotech), and Neonatal Cardiomyocyte Isolation Kit (130-105-420, Miltenyi Biotech), as per the manufacturer's informations. The cells were counted and plated on laminin-coated coverslips.

Cloning

Mouse and human RBM20 were cloned from mouse and human cDNA, respectively. Flag-tagged RBM20 constructs were created by PCR using Q5 polymerase (NEB) with primers listed in Table S1. Ligation was performed using T4 DNA ligase (NEB). Constructs were Sanger sequenced and used as templates for introducing the DupC mutation. Mutagenesis was performed using the QuikChange XL Site-Directed Mutagenesis Kit (Agilent) according to the manufacturer's instructions using the primers given in Table S1.

Transfection of HEK293 Cells

HEK293 cells were grown in DMEM medium with 10% FBS in a 5% CO_2 incubator. GeneJammer transfection reagent (Agilent) was used for transfection, and 1 µg of pcDNA-FLAG-*RBM20* or pcDNA-FLAG-*RBM20*-DupC was transfected per well in a 6-well plate. Empty pcDNA vector was used as a negative control. Data from WT RBM20 and RBM20-DupC protein and RNA expression are presented as mean±SEM from biological replicates (n=6).

Splicing Reporter Assay

HEK293 cells were plated in 96-well plates and transfected at 50% confluency using PEI40 at a DNA-to-PEI40 ratio of 1:3, with a total of 200 ng plasmid DNA. The DNA mixture consisted of 1 ng of the *TTN*-IG Ex241-243 splice reporter and a 20-fold molar excess of *RBM20* expression plasmids or the control plasmid pcDNA3.1 (Invitrogen, Cat V79520). Plasmids and PEI40 were preincubated for 15 minutes in serum-free medium before being added to the cells. Each transfection was repeated 10×. After 60 hours, cell viability was assessed using PrestoBlue (Thermo Fisher Scientific, Cat A13261). At the same time point, luciferase activity was measured with the Dual-Luciferase Reporter Assay System (Promega) on an Infinite M200 Pro plate reader (TECAN). Firefly luciferase activity was normalized to Renilla luciferase and expressed relative to WT *RBM20*-transfected cells. Data are presented as mean±SEM from biological replicates (n=8). Statistical significance was determined by 1-way ANOVA with Bonferroni posttest.

Cycloheximide Pulse-Chase Assay

HEK293 cells were transfected with FLAG-WT and FLAG-DupC as described above. Twenty-four hours post-transfection, cells were subjected to either 50 µg/mL cycloheximide or DMSO as a vehicle control. Cells were collected at 0, 1, 3, 6, 12, and 24 hours after addition of cycloheximide. Data were collected from 2 separate experiments.

In Vitro Transcription

In vitro transcription was performed using the T3 Messenger Max kit (Thermo Fisher). pT3Ts-containing clones were digested with *Xba*I to linearize the plasmid. Linear plasmids were eluted from gel, and 300 ng of DNA was taken as template to perform in vitro transcription as per the manufacturer's protocol. The transcribed RNAs were polyadenylated with *E. coli*. Poly A polymerase (NEB, M0276L). The polyadenylated RNA was precipitated using LiCl assisted precipitation as per the instructions provided by the manufacturer.

Transfection of NRCMs

Lipofectamine MessengerMAX mRNA Transfection Reagent (Thermo Fisher) was used to transfect 500 ng of RNA per well in a 24-well plate. Lipofectamine and RNA mix were prepared in Opti-MEM medium as per the manufacturer's instructions. The cells were incubated with RNA-lipofectamine mix for 24 hours. mRNA of GFP was used as positive control for transfection. Cells were collected for downstream analysis after 24 hours.

Immunocytochemistry

Cells were fixed in 4% paraformaldehyde for 15 minutes, washed 3× in PBS, and permeabilized in 0.1%Triton X-100/

PBS for 10 minutes. Cells were blocked in 4% normal goat serum for 1 hour at room temperature and then incubated with primary antibody in 4% normal goat serum overnight at 4 °C. Secondary antibody incubation occurred in 4% normal goat serum for 1 hour at room temperature. Nuclear staining was performed as a last step using DAPI. Coverslips were then mounted on glass slides with Vectashield HardSet mounting medium (H-1400-10), and images were captured using confocal microscopy (Leica Mica). Primary antibodies used were: rabbit anti-FLAG (1:250, Sigma F7425), mouse anti-FLAG (Sigma F1804-1MG), rabbit anti-RBM20 (1:250, Sigma HPA0377703), rabbit anti-Myc (1:200, Cell Signaling, 2278S), mouse anti-Actinin (1:400, Sigma A7811). Alexa Fluor 488, Alexa Fluor 594, and Alexa Fluor 647 conjugated antibodies (1:250, Invitrogen) were used as secondary antibodies.

Western Blotting

Cells were lysed in ice-cold RIPA-buffer (50 mM Tris-HCl, 150 mM NaCl, 1% NP-40, 0.2% sodium deoxycholate, 0.1% SDS) supplemented with DTT, PMSF, and protease inhibitor cocktail (Thermo). Cell lysates were cleared by centrifuging at 14 000×*g* for 10 minutes at 4 °C. Western blotting was performed according to standard protocols. Briefly, protein concentrations were determined using the BCA protein assay (Pierce), and proteins were resolved by SDS-PAGE and transferred to polyvindyline difluoride membranes (Merck). Polyvindyline difluoride membranes were incubated overnight at 4 °C with the following primary antibodies: rabbit anti-FLAG (1:1000, Thermo Scientific), rabbit anti-RBM20 (1:1000, HPA0377703, Sigma), and mouse anti-GAPDH (1:5000, MAB374, Sigma). Horseradish peroxidase-conjugated secondary antibodies (Biozol) were used for detection and incubated for 1 hour at room temperature. Western blots were developed with ECL prime Western blotting detection reagent (Santa Cruz), and images were acquired using the Vilber Fusion FX (Vilber). Densitometric analysis of Western blots was performed using ImageJ software.

RNA Isolation and q(RT)-PCR

RNA was isolated using TRIzol (Invitrogen) according to the manufacturer's protocol. Subsequently, 1 µg RNA was used for cDNA synthesis using reverse transcriptase (Steinbrenner Laborsysteme GmbH). Reverse transcriptase-polymerase chain reaction was performed using Taq polymerase with primers listed in Table S2. Quantitative polymerase chain reaction was performed on a LightCycler 480 (Roche) using SYBR green premix (Applied Biosystems). Analysis of quantitative polymerase chain reaction data was performed using LinRegPCR analysis software.[19] Primers used for quantitative polymerase chain reaction are provided in Table S2. Gene expression was normalized to the geometric mean of Gapdh and Hprt expression.

RNA Sequencing

Total RNA was isolated with TRIzol (Life Technologies) according to the manufacturer's instructions. RNA integrity was verified with the Agilent Bioanalyzer (Agilent Biotechnologies) before RNA-seq libraries were prepared using the SMART-Seq Total RNA Pico Input Kit (634354, Takara Bio) with the Unique Dual Index Kit (634752, Takara Bio). Libraries were then sequenced on an Aviti sequencer (Element Biosciences). Sequencing reads were mapped to the GENCODE GRCh38 reference genome (release 45, Ensembl 111) using RNA STAR (v2.7.11b) on the Galaxy platform (https://galaxyproject.org).[20] Gene-level counts were generated with featureCounts (v2.1.1). We performed principal component analysis in DESeq2 on the VST-transformed expression matrix. Raw counts were first normalized using DESeq2 size factors, then principal component analysis was computed on centered VST values (Euclidean covariance-based decomposition) for the most variable genes. The percentage of variance explained by each principal component was taken from the DESeq2 output and used to label the principal component analysis axes in ggplot2. Differential gene expression between DupC and WT groups was analyzed in R using DESeq2 (v1.42.1)[21] Multiple testing correction was applied using the Benjamini-Hochberg procedure. Genes were considered significantly differentially expressed if they exhibited a (|log2FC| >0.5) with an adjusted $P<0.05$. Gene ontology analysis was subsequently performed using ClusterProfiler (v4.14.6).[22] To investigate alternative splicing differences, we applied rMATS-turbo (turbo_v4_1_2) on a Linux environment.[23] Five classes of splicing events were examined: exon skipping (SE), mutually exclusive exons, alternative 3′ splice sites, alternative 5′ splice sites, and retained introns. Among these, SE events identified using both junction and exon counts were selected for downstream analysis. Exon inclusion differences between conditions were quantified using ΔPSI (percent spliced-in), calculated as ΔPSI=PSI(DupC) − PSI(WT). SE events were considered significant when the *P* value was <0.01 and ΔPSI was >0.1. Data visualization and statistical plots were generated in R using the ggplot2, pheatmap, dplyr, and tidyr packages.

Statistics

GraphPad Prism was used for data analysis and statistics. Data are presented as mean±SEM, and were analyzed with appropriate statistical tests, as indicated in the respective figure legends. A value of $P<0.05$ was considered statistically significant.

RESULTS

Identification of a Novel *RBM20* Variant

A 50-year-old male patient presented with mitral valve prolapse and severe mitral regurgitation, and developed DCM immediately after mitral valve repair. Family history showed multiple family members with DCM and sudden cardiac death (Figure 1A). Targeted clinical cardiomyopathy and arrhythmia gene-panel sequencing of the proband identified a novel truncating variant in *RBM20*, which constituted the duplication of a cytosine at position c.1222 (hereafter called *RBM20*-c.1222DupC). The father of the patient was also found to be a carrier of the *RBM20*-c.1222DupC variant. This duplication leads to a frameshift and a premature stop codon 8 amino acids downstream of the variant (p.Leu408ProfsX8; Figure 1B). The patient experienced multiple runs of nonsustained ventricular tachycardia lasting up to 24 beats. Cardiac MRI showed a left ventricular ejection

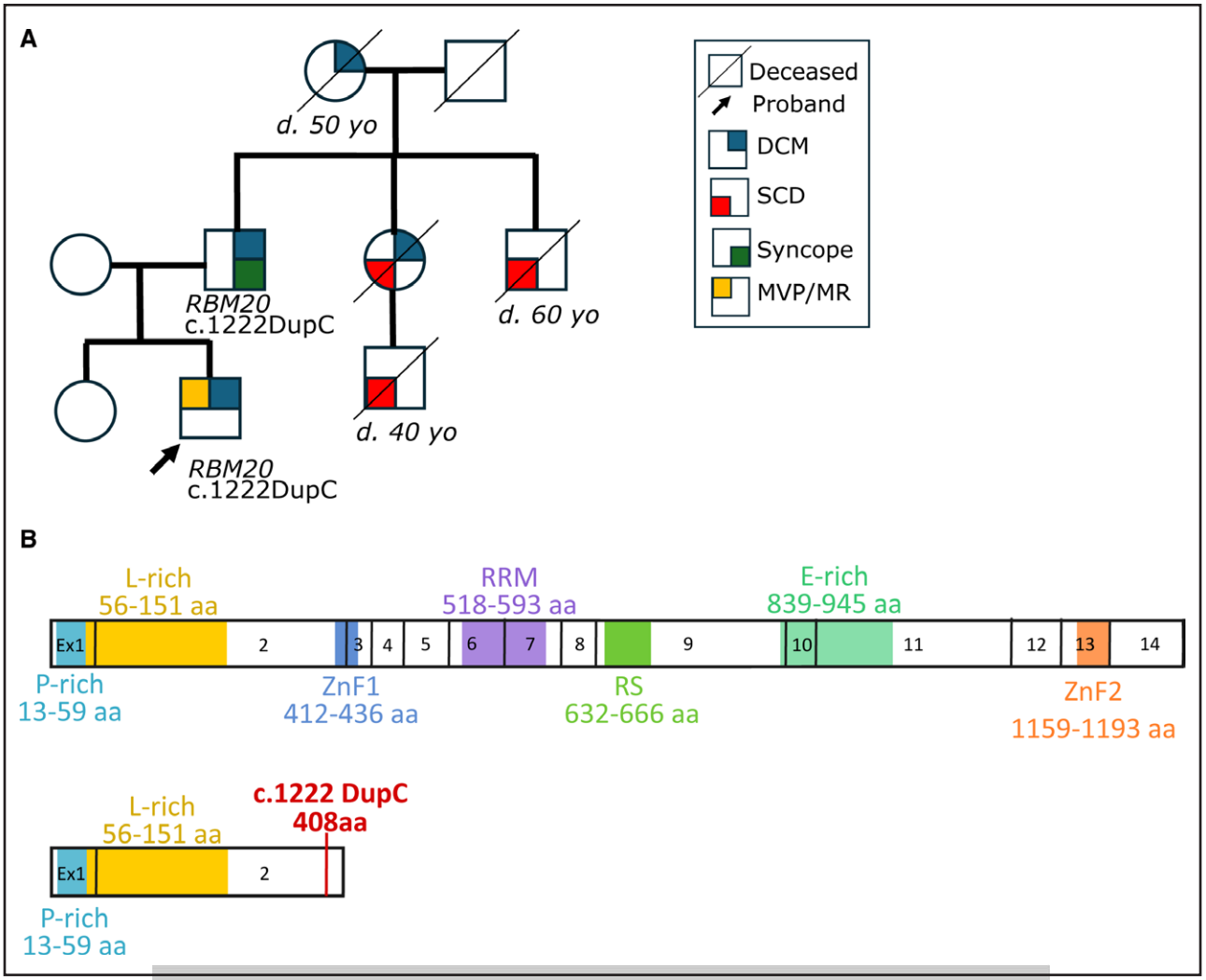

Figure 1. Identification of the *RBM20*-c.1222DupC variant.
A, Family pedigree of the proband with the *RBM20*-c.1222DupC variant. Proband is marked by arrow. **B**, Schematic visualization of RBM20 (RNA binding motif protein 20) protein structure, numbers represent exons and known functional domains are denoted in different colors. Top diagram represents the full-length RBM20 and bottom diagram represents truncated RBM20-c.1222DupC protein with the position of the variant marked with a red vertical line. DCM indicates dilated cardiomyopathy; MR, mitral regurgitation; MVP, mitral valve prolapse; and SCD, sudden death.

fraction of 39%, moderate left ventricular enlargement, and delayed gadolinium enhancement of both the papillary muscle and the mesocardium of the lateral wall. A primary prevention implantable cardioverter defibrillator was implanted at that time, and the patient was started on guideline-directed medical therapy for heart failure. No additional major arrhythmias or heart failure hospitalizations were recorded since diagnosis.

Protein Stability of the Truncated RBM20-DupC Protein Is Decreased as Compared With the WT RBM20 Protein

To determine whether the *RBM20*-c.1222DupC variant has an effect on translation, we generated FLAG-tagged constructs of mouse and human WT *RBM20* and *RBM20*-DupC, and validated the variant using Sanger sequencing (Figure 2A). We then transfected FLAG-tagged human and mouse WT *RBM20* and *RBM20*-DupC into HEK293 cells. We measured the transcript levels of both the WT *RBM20* and *RBM20*-DupC and found no significant difference (Figure 2B). Immunoblotting revealed that *RBM20*-DupC produced a protein of ≈55 kDa, whereas the full-length WT RBM20 showed its typical size of 180 kDa (Figure 2C). Densitometric analysis revealed ≈50% reduction for mouse and ≈70% reduction for human truncated RBM20 compared with the respective full-length protein, suggesting a decrease in protein stability (Figure 2D). We then performed a cycloheximide pulse-chase assay, and expressed WT *RBM20* or *RBM20*-DupC in HEK293 cells, after which we isolated proteins at different timepoints. The WT RBM20 protein remained stable whereas RBM20-DupC progressively decreased over time (Figure 2E and

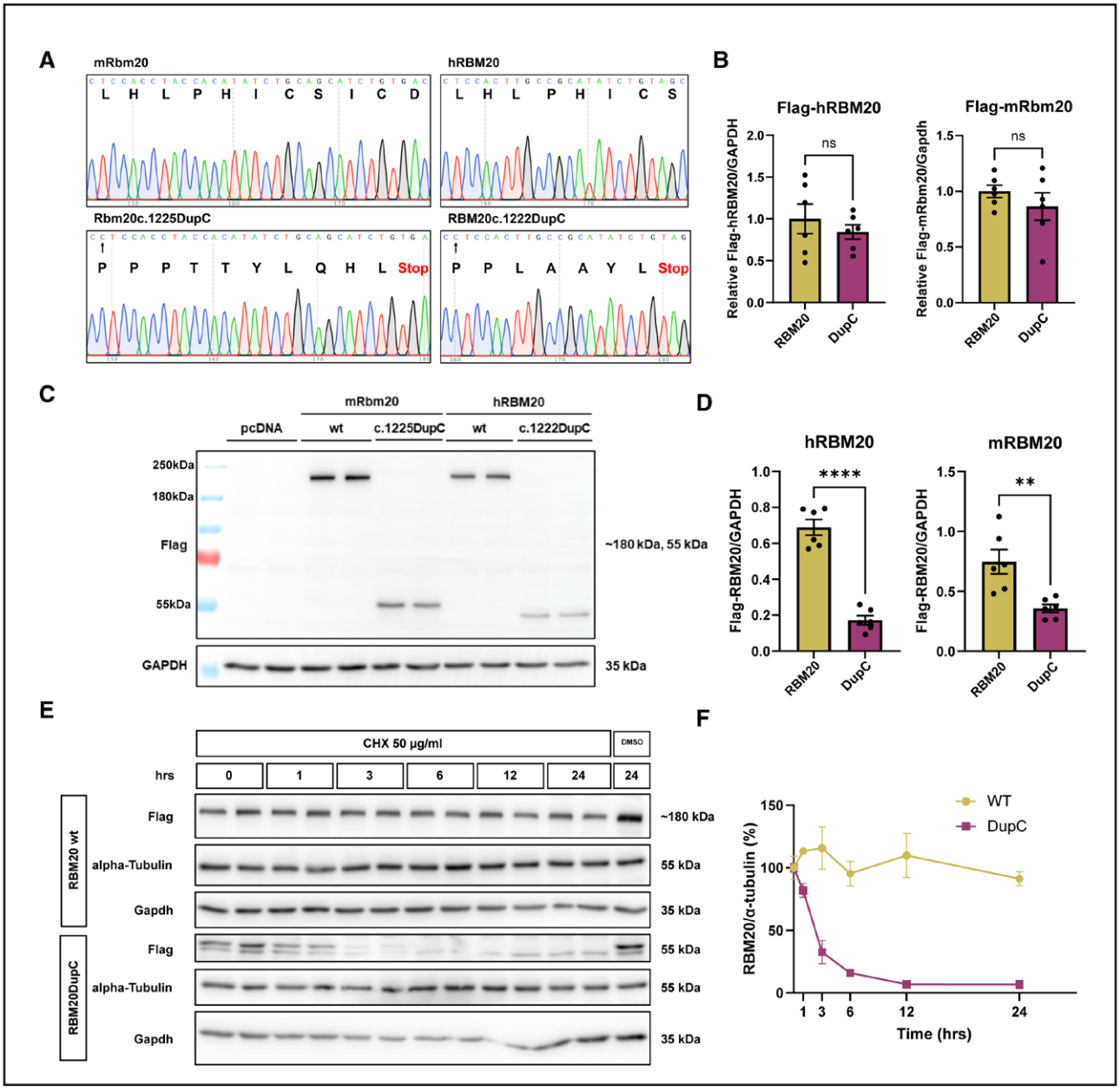

Figure 2. The truncated RBM20 (RNA binding motif protein 20)-DupC protein is less stable.
A, Sanger sequencing of the mouse (**left**) and human (**right**) wild-type (WT; **top**), and DupC (**bottom**) *RBM20* constructs. Amino acid sequence is added underneath the nucleotide sequence. The red line in the bottom panels indicates the site of c.1222DupC variant. **B**, Expression of mouse and human *RBM20* mRNA transcript in HEK293 cells transfected with equal amounts of plasmid with mouse or human WT-*RBM20* or *RBM20*-DupC (n=6/condition). **C**, Representative immunoblotting of FLAG-tagged full-length RBM20 and RBM20-DupC in HEK293 cells. **D**, Densitometric analysis of the FLAG-tagged RBM20 and FLAG-tagged RBM20-DupC normalized to GAPDH intensity (n=6/condition). ***P*<0.01, *****P*<0.0001. Significance was tested using a 2-tailed *t* test. **E**, Immunoblotting of FLAG-tagged WT RBM20 and RBM20-DupC following a cycloheximide (CHX) pulse-chase assay. **F**, Quantification of FLAG-tagged protein levels normalized to α-tubulin (n=4/timepoint). Protein amounts at 0 hour are set to 100% for both WT RBM20 and RBM20-DupC. Data collected from 2 independent experiments.

2F). This confirms that protein stability of the truncated RBM20-DupC protein is decreased.

RBM20-DupC Shows Both Nuclear and Cytoplasmic Localization

To assess the localization of the RBM20-DupC, we overexpressed FLAG-tagged human and mouse WT RBM20 and RBM20-DupC in NRCMs. Both human and mouse WT RBM20 demonstrated nuclear localization with the characteristic bipunctate pattern (Figure 3A and 3B). In contrast, RBM20-DupC showed both nuclear and cytoplasmic localization. Interestingly, a portion of the nuclear-localized RBM20-DupC protein appeared to colocalize with the WT RBM20. To further confirm this colocalization, we co-transfected NRCMs with FLAG-tagged

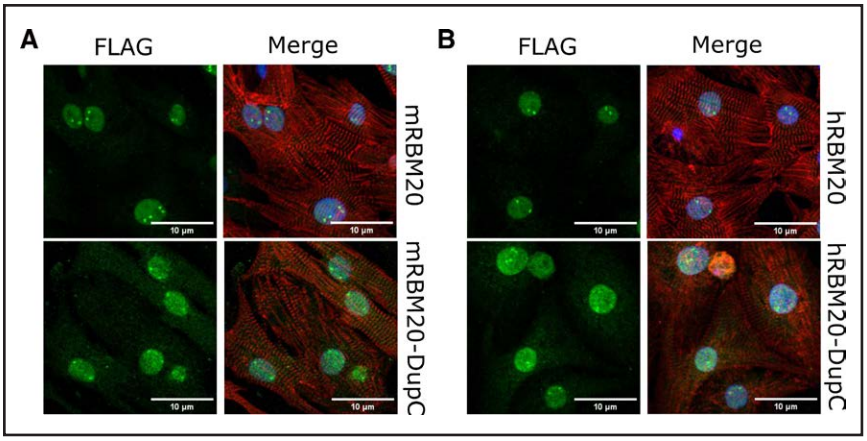

Figure 3. RBM20 (RNA binding motif protein 20)-DupC shows both nuclear and cytoplasmic localization.
A, Immunofluorescence of neonatal rat cardiomyocytes (NRCMs) transfected with mouse FLAG-tagged *Rbm20* or FLAG-tagged *Rbm20*-DupC. FLAG is stained in green, α-actinin in red, and DAPI in blue. Scale bar is 10 µm. **B**, Immunofluorescence of NRCMs transfected with human FLAG-tagged *RBM20* or FLAG-tagged *RBM20*-DupC. FLAG is stained in green, α-actinin in red, and DAPI in blue. Scale bar is 10 µm.

human *RBM20*-DupC and Myc-tagged human WT *RBM20*. Confocal imaging revealed that RBM20-DupC was indeed present in both the cytoplasm and nucleus and, within the nucleus, it colocalized with WT RBM20 (Figure S1).

RBM20-DupC Truncated Protein Does Not Have Residual Splicing Repressor Activity Nor Does It Act as a Dominant Negative

To check the splicing regulatory activity of RBM20-DupC, we used a previously reported splicing assay in HEK293 cells.[24] We overexpressed human and mouse WT *RBM20* and *RBM20*-DupC in the presence of a *TTN* splicing reporter and measured the ratio of luciferase to Renilla activity (Figure 4A). While WT RBM20 skipped the Fluc-containing exon, RBM20-DupC was not sufficient to repress exon 242-Fluc (Figure 4B and 4C). In addition, upon transfecting the cells with increasing concentrations of *RBM20*-DupC, we observed no change in the splicing regulatory activity of the WT RBM20 (Figure 4B and 4C). This indicates that RBM20-DupC does not have a dominant-negative effect on the splicing regulatory activity of the WT RBM20 protein.

hiPSC-CMs Engineered to Carry *RBM20*-c.1222DupC Display Splicing Abnormalities and Calcium-Handling Defects

To model the patient's condition, we introduced the *RBM20* c.1222DupC variant in a heterozygous manner into hiPSCs from a healthy individual using PE3. The presence of both the WT and DupC alleles was confirmed in differentiated cardiomyocytes (Figure 5A and 5B). Immunostaining for α-actinin and cTnT (encoded by *TNNT2*) revealed a striated pattern in both WT and DupC±hiPSC-CMs, consistent with proper sarcomeric organization and successful differentiation into cardiomyocytes (Figure 5C). Western blot analysis showed a ≈50% reduction in WT RBM20 protein in heterozygous cardiomyocytes compared with WT controls, while *RBM20* mRNA levels remained unchanged (Figure 5D and 5E). RNA sequencing revealed that *RBM20* mRNA transcripts in the heterozygous DupC hiPSC included both WT and DupC transcripts, which we could confirm by Sanger sequencing (Figure 5F and Figure S2A). This suggests that the DupC transcript is not subjected to nonsense mediated decay (NMD), but instead that the c.1222DupC variant may lead to reduced protein stability. We next assessed the splicing of known RBM20 targets. In DupC± hiPSC-CMs, aberrant splicing was observed for titin (*TTN*) and *RYR2* (Figure 5G). In addition, we measured mRNA expression of multiple cardiomyocyte markers and found that the expression of *GATA4* was similar between WT and DupC±hiPSC-CMs, while *TNNT2* was slightly decreased (Figure 5H). Moreover, even though MYH7 is the dominant myosin protein in adult human cardiomyocytes, DupC± hiPSC-CMs displayed a shift toward MYH6 expression (Figure 5I). We then investigated calcium handling and found an increase in diastolic and systolic calcium, an increased calcium transient amplitude, an increased rise velocity, and a decreased decay time in DupC± hiPSC-CMs (Figure 5J). These results are in line with published findings on *Rbm20* KO cardiomyocytes and are likely to contribute to the arrhythmogenic phenotype of *RBM20* variant carriers.[17]

Transcriptomic Analysis Reveals Missplicing of RBM20 Targets and a Shift Toward a Disease-Like State

Transcriptome profiling by RNA sequencing revealed different clustering of WT and DupC±hiPSC-CMs, and widespread gene expression changes, with 1683 genes upregulated and 1768 genes downregulated (|log2FC| >0.5, adjusted P <0.05; Figure 6A and 6B; Table S3). KEGG pathway enrichment analysis showed that downregulated genes were enriched for categories related to hypertrophic cardiomyopathy, whereas upregulated genes were associated with extracellular matrix receptor interactions and Wnt signaling (Figure 6C). Gene

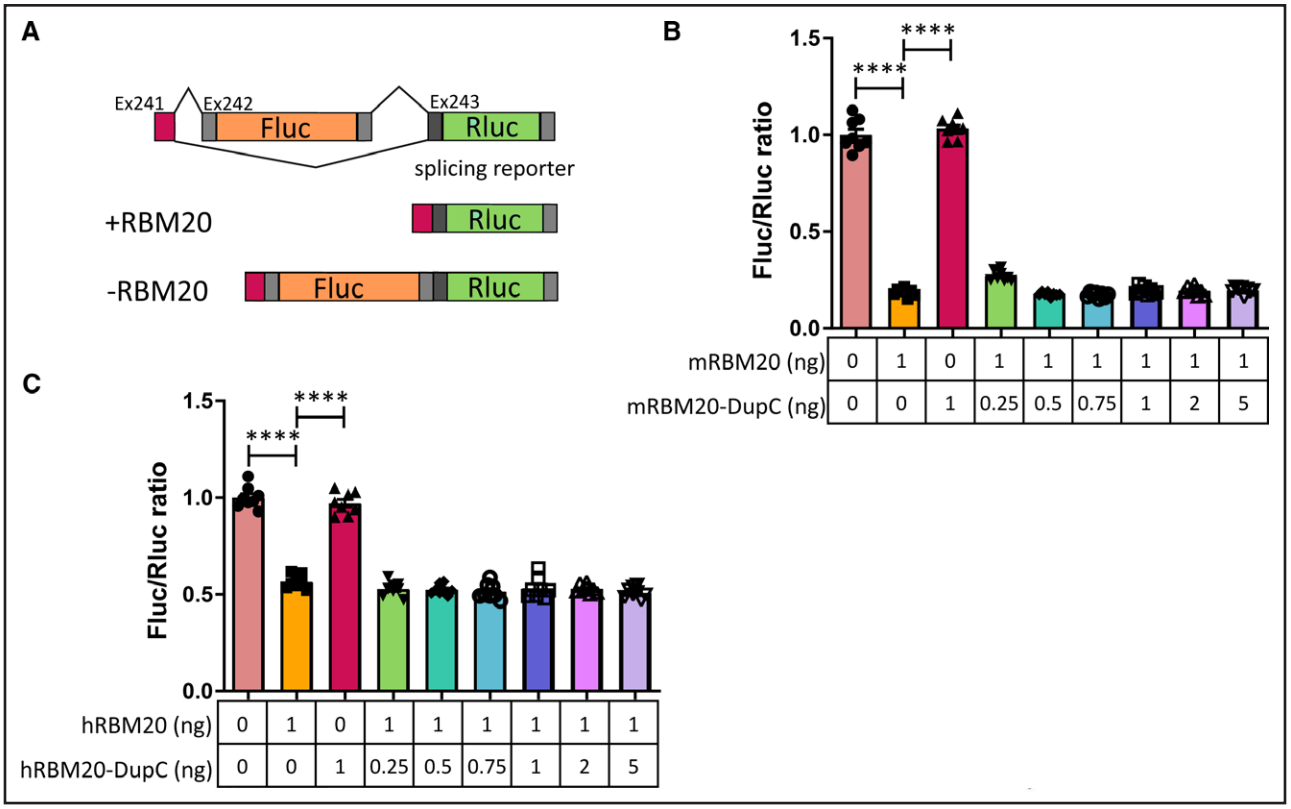

Figure 4. RBM20 (RNA binding motif protein 20)-DupC does not have residual splicing regulatory activity and does not act as a dominant negative.

A, Schematic drawing of the *TTN* splicing reporter. **B**, Ratio of Firefly luciferase to Renilla luciferase in HEK293 cells transfected with empty vector control, mouse *Rbm20*, mouse *Rbm20*-DupC, or both (n=8/condition). **C**, Ratio of Firefly luciferase to Renilla luciferase in HEK293 cells transfected with empty vector control, human *RBM20*, human *RBM20*-DupC, or both (n=8/condition). ****P<0.0001. Significance was tested using a 1-way ANOVA with Bonferroni post hoc test.

set enrichment analysis further revealed that downregulated transcripts in cellular component categories were enriched for genes involved in Z-disc organization, contractile fibers, and costameres, while upregulated transcripts included extracellular matrix- and collagen-related genes (Figure 6D; Figure S3; Table S4). Terms related to Wnt signaling were also enriched in molecular function and biological process categories with decreased expression of genes involved in lipid homeostasis (Figure S3A and S3B). These results indicate that DupC±hiPSC-CMs suggest a shift from a more contractile to a remodeling/fibrotic state. We then used rMATS-turbo, an established method for quantitative analysis of differential splicing events, to compare splicing changes between WT and DupC±hiPSC-CMs across 5 distinct categories: SE, retained introns, mutually exclusive exons, and usage of alternative 3′ splice site or alternative 5′ splice sites. To compute the differences in AS, we used junction and exon body read counts for each AS event. Significant changes were detected across all 5 categories, with the most extensive alterations observed in the SE and mutually exclusive exon types. Specifically, 90 events showed higher exon inclusion in WT, whereas 117 SE events exhibited higher exon inclusion in DupC±hiPSC-CMs. Similarly, 10 mutually exclusive exon events were more included in WT and 21 in DupC± (Figure 6E). Given that SE events were the most affected, we calculated ΔPSI (percent spliced-in) values using junction and exon counts to measure the exon inclusion differences between WT and DupC± (P<0.01 and|ΔPSI|> 0.1; Table S5). Among the top 50 significantly altered SE events (P<0.05), several well-established RBM20 targets, including *TTN*, *CAMK2D*, and *RYR2* were identified (Figure 6F). Other splicing targets such as *OBSCN*, *MTMR2* and *CACNA1G* also showed differential splicing (Table S5). Overall, we demonstrate that the *RBM20*-c.1222DupC variant leads to missplicing of many known RBM20 targets and a shift in the transcriptome toward a more disease-like state.

DISCUSSION

Variants in *RBM20* are a well-established cause of familial DCM, and several pathogenic variants have been reported in patients. Here, we report a novel heterozygous *RBM20* variant, specifically a duplication at nucleotide 1222 (c.1222DupC), identified in a patient with mitral valve prolapse and late-onset, mild DCM. This

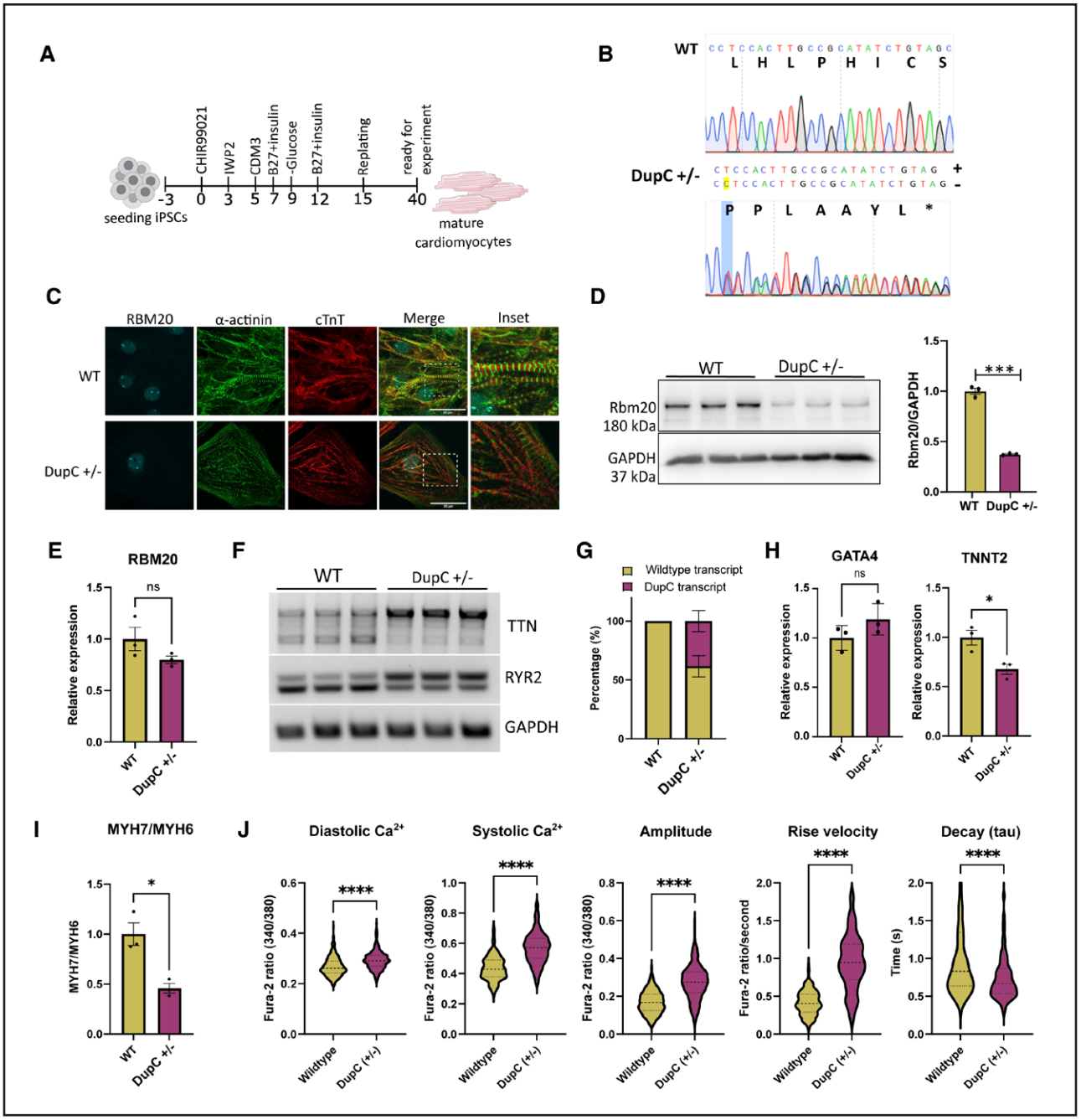

Figure 5. ***RBM20*** **c.1222DupC human induced pluripotent stem cell-derived cardiomyocyte (hiPSC-CM) present with splicing and calcium-handling abnormalities.**

A, Schematic representation of the workflow used to differentiate hiPSCs to cardiomyocytes. **B**, Sanger sequencing of the *RBM20*-DupC (±) hiPSC-CM. In the DupC (±) panel, the top nucleotide sequence represents the wild-type (WT) sequence, and the bottom nucleotide sequence represents the mutated sequence with the duplicated C marked in yellow. Amino acid sequence is added underneath the nucleotide sequence. **C**, Immunofluorescence of WT and Dupc (±) hiPSC-CM stained using anti-RBM20 (RNA binding motif protein 20; blue), anti-α-actinin (green), and anti-TNNT2 (red). Scale bar=30 µm. **D**, Immunoblotting of the cell lysate from WT and DupC (±) lines using anti-RBM20 antibody, the densitometric quantification presented as the bar graph (n=3/condition). **E**, qPCR analysis of *RBM20* in WT and DupC (±) hiPSC-CM (n=3/condition). **F**, Percentage of WT and DupC transcripts in RNA-seq of WT and DupC iPSC-CM. **G**, RT-PCR of RBM20 splice targets, GAPDH is used as control. **H**, qPCR analysis of *GATA4* and *TNNT2* in WT and DupC (±) hiPSC-CM (n=3/condition). **I**, Ratio of *MYH7* to *MYH6* in in WT and DupC (±) hiPSC-CM (n=3/condition). **J**, Violin plots representing diastolic calcium, systolic calcium, Ca^{2+} transient amplitude, rise velocity, and Tau (decay time) of WT and DupC hiPSC-CM (n=297/condition). **P*<0.05 ***P*<0.01, *****P*<0.0001. Significance was tested using a 2-tailed *t* test.

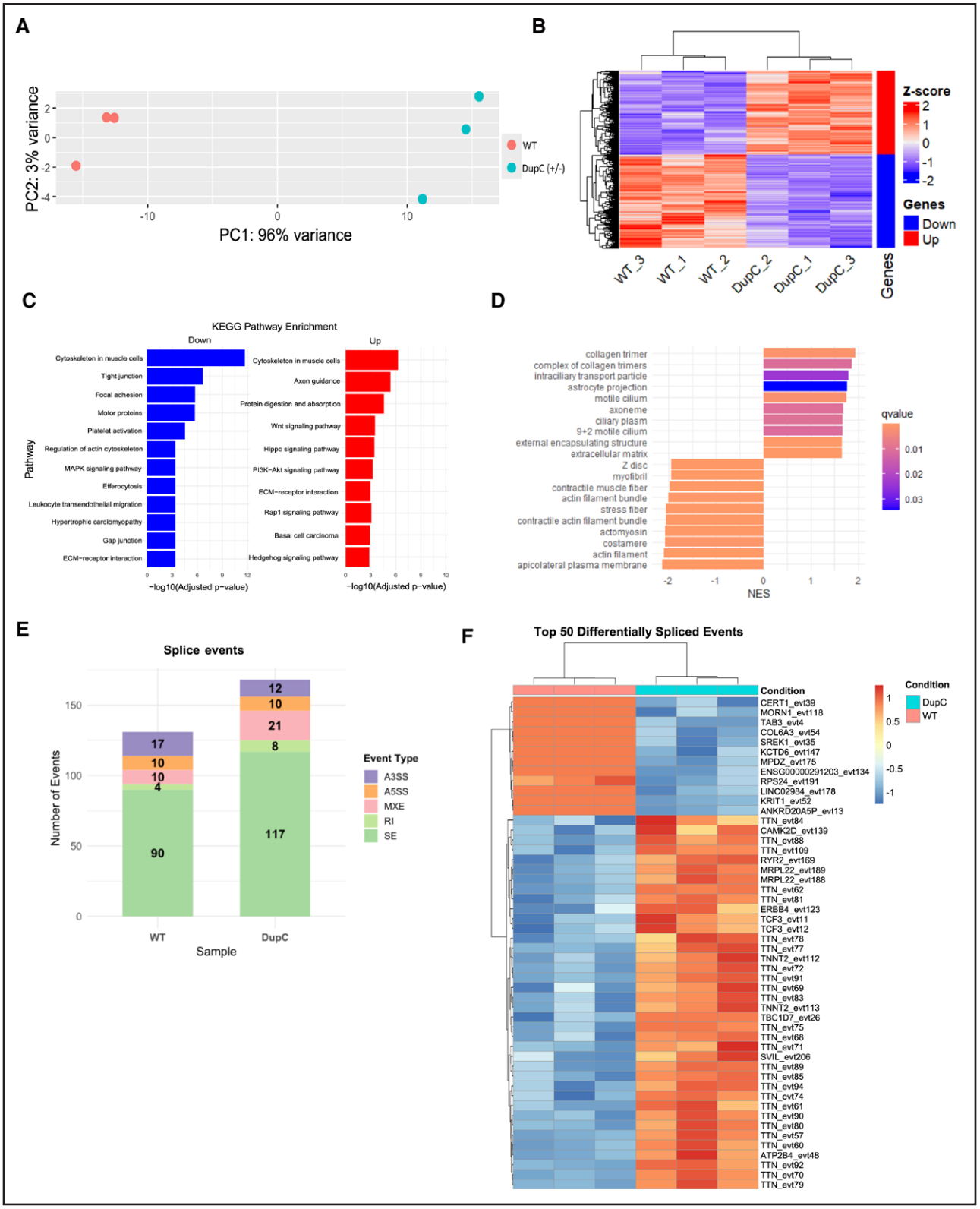

Figure 6. Transcriptomic analysis on *RBM20* c.1222DupC human induced pluripotent stem cell-derived cardiomyocyte (hiPSC-CM). **A**, Principal component analysis (PCA) plot of the reads from wild-type (WT) and DupC (±) hiPSC-CM. **B**, Heat map showing the differentially expressed genes (DEGs) in WT and DupC (±) hiPSC-CM. **C**, KEGG pathway enrichment analysis of the DEGs of DupC (±) hiPSC-CM. **D**, Gene set enrichment analysis (Cellular component) of the DEGs of DupC (±) hiPSC-CM. **E**, Number of splice events detected in WT and DupC (±) hiPSC-CM events with an FDR <0.01 and ΔPSI >0.1 were included. **F**, Heatmap of top 50 differential splicing events between WT and DupC (±) hiPSC-CM. A3SS indicates alternative 3′ starting site; A5SS, alternative 5′ starting site; MXE, mutually exclusive exons; RI, intron retention; and SE, exon skipping.

is distinct from most reported *RBM20* variants, which are predominantly missense single-nucleotide substitutions. Interestingly, the patient developed mitral valve prolapse before the onset of DCM, which is unusual, as mitral valve prolapse is not a recognized phenotype in RBM20-associated cases. However, a GWAS (genome-wide association study) recently identified an intronic variant in *RBM20* associated with increased mitral valve prolapse risk, raising the possibility that *RBM20* variation may influence mitral valve biology.[25] Most of the early reported variants in *RBM20* are located in the RS domain and are associated with a severe and early-onset DCM phenotype. However, there are now several reports showing that variants in other domains can also give rise to DCM. For example, patients with the V535I variant in exon 6 within the RNA recognition motif domain and the R716Q variant located just outside the RS domain showed delayed development of DCM compared with the RS-domain variants.[26] This difference in disease severity between the RS-domain versus non–RS-domain variants indicates that missplicing alone is not sufficient to fully explain the disease phenotype in patients with RS-domain variants. Although *RBM20* truncating variants have been reported less frequently, emerging data suggest that these variants can lead to late-onset DCM along with an elevated risk of ventricular arrhythmias.[14,27] For example, the *RBM20* Q373fs truncating variant has recently been reported in a patient who died suddenly. Postmortem evaluation showed no structural remodeling, and therefore without structural remodeling this phenotype was attributed to missplicing of calcium-handling genes.[16] In addition, *RBM20*tvs independently predict major ventricular arrhythmia risk, independent of the degree of structural remodeling.[15] Consistent with these insights, the patient in this study developed late-onset DCM and experienced several episodes of nonsustained ventricular tachycardia.

Overexpression of the DupC transcript produces a truncated protein that lacks splicing regulatory activity and does not exhibit a dominant-negative effect on the WT RBM20 protein, suggesting that this variant may lead to haploinsufficiency. Based on our overexpression and localization studies, we can conclude that the *RBM20* c.1222DupC allele is capable of translation. However, we cannot confirm whether this truncated protein is stably expressed or detectable in patient tissue. Since the variant introduces a premature termination codon, it is possible that the majority of *RBM20*-c.1222DupC transcripts undergo NMD, thereby reducing *RBM20* transcript and protein dosage in vivo. Overexpression experiments did not reveal transcript reduction, but these constructs contained only the coding sequence and not the exon junctions of *RBM20*, and would therefore bypass NMD. Importantly, in the *RBM20*-c.1222DupC hiPSC-CMs, we did not observe a decrease in the *RBM20* mRNA levels and confirmed the presence of both the WT and DupC transcripts, which suggests that the DupC transcript is not subjected to NMD in a human cell model.

Recently, Methawasin and colleagues[28] showed that downregulating mutant RBM20 is beneficial in a mouse model with the RS-domain variant *Rbm20*-R639G. However, our data show that loss of RBM20 still leads to disease, which means that RBM20 downregulation as a therapeutic option should be carefully evaluated. This is underscored by the fact that *Rbm20* KO models likewise have cardiac dysfunction.[17,24] RBM20 typically localizes to the nucleus, forming 2 characteristic puncta that correspond to the sites of *TTN* transcription which are crucial for RBM20 function.[29] RBM20's ability to localize to these foci is mediated by its RNA recognition motif domain, and this spatial organization is thought to facilitate efficient RBM20-mediated splicing regulation of its targets.[29–31] Furthermore, previous studies on *RBM20* RS-domain variants have demonstrated that the RS domain is essential for the proper nuclear localization of RBM20.[6,7,32,33] Variants in this domain inhibit the interaction of RBM20 with TNPO3, its nuclear transporter, and inefficient interaction between RBM20 and TNPO3, at least in part, is responsible for this mislocalization.[6] Interestingly, when a nuclear localization signal is artificially introduced to an RS-domain variant, it restores normal splicing of RBM20 targets.[6] Given what is known about the function of these domains, it is surprising that the truncated RBM20-DupC protein is localized in both the nucleus and cytoplasm, even though it only contains the N-terminal leucine/proline-rich domain. Furthermore, a portion of the nuclear-localized DupC protein colocalizes with WT RBM20. This raises important questions about the role of the N-terminal region of RBM20 in protein localization and function, as it appears to contain an uncharacterized mechanism for nuclear localization. In summary, we identify a novel truncating *RBM20* variant (c.1222DupC) that causes DCM through haploinsufficiency rather than through dominant-negative splicing defects. In addition, the unexpected nuclear localization of the truncated protein suggests the presence of an unrecognized function of the N-terminal leucine/proline-rich domain of RBM20. Together, these findings broaden the mechanistic spectrum of RBM20 cardiomyopathy and highlight dosage sensitivity as a critical disease determinant.

ARTICLE INFORMATION

Received September 9, 2025; accepted April 4, 2026.

Affiliations

Medical Faculty Heidelberg, Institute of Experimental Cardiology, Heidelberg University, Germany (P.P., Z.G., E.K., L.K., M.M.G.v.d.H.). Department of Internal Medicine VIII (P.P., Z.G., E.K., L.K., M.M.G.v.d.H.), and Department of Internal Medicine III (A.A., R.K., T.S.), Heidelberg University Hospital, Germany. German Centre for Cardiovascular Research (DZHK), Partner Site Heidelberg/Mannheim, Germany (P.P., Z.G., A.A., R.K., T.S., M.M.G.v.d.H.). Helmholtz-Institute for Translational AngioCardioScience (HI-TAC) of the Max Delbrück Centre for Molecular Medicine in the Helmholtz Association (MDC) at Heidelberg University, Germany (P.P., Z.G., E.K., L.K., M.M.G.v.d.H.). Stanford Centre for Inherited Cardiovascular Disease and Department of Medicine,

Stanford School of Medicine, CA (Y.H., F.B., V.N.P.). Translational Cardiology and Functional Genomics, Max Delbrück Centre for Molecular Medicine, Germany (M.G.). DHZC, Charite Universitätsmedizin Berlin, Germany (M.G.). German Centre for Cardiovascular Research (DZHK), Partner Site Berlin, Germany (M.G.).

Acknowledgments

The authors gratefully acknowledge J. Fröhlich for technical help, and the data storage service SDS@hd which is supported by the Ministry of Science, Research and the Arts Baden-Württemberg (MWK) and the German Research Foundation (DFG) through grant INST 35/1503-1 FUGG.

Sources of Funding

This publication was supported through state funds approved by the State of Baden-Württemberg for the Innovation Campus Health and Life Science Alliance Heidelberg Mannheim, through the Helmholtz Institute for Translational AngioCardioScience (HI-TAC), and through grants from the Deutsche Forschungsgemeinschaft (DFG, German Research Foundation) with grant number HO 6446/1, and SFB1550—Project ID 464424253: Collaborative Research Center 1550 (CRC1550) Molecular Circuits of Heart Disease to MvdH. Dr Pant was supported by an Interinstitutional Postdoc fellowship from the Health and Life Science Alliance Heidelberg Mannheim. Dr Gotthardt was supported by the European Research Council (ERC-Adv) and the Deutsche Forschungsgemeinschaft (DFG, German Research Foundation).

Disclosures

None.

Supplemental Material

Tables S1–S5
Figures S1–S3

REFERENCES

1. Lennermann D, Backs J, van den Hoogenhof MMG. New insights in RBM20 cardiomyopathy. *Curr Heart Fail Rep*. 2020;17:234–246. doi: 10.1007/s11897-020-00475-x
2. Gregorich ZR, Zhang Y, Kamp TJ, Granzier HL, Guo W. Mechanisms of RBM20 cardiomyopathy: insights from model systems. *Circ Genom Precis Med*. 2024;17:e004355. doi: 10.1161/CIRCGEN.123.004355
3. Briganti F, Sun H, Wei W, Wu J, Zhu C, Liss M, Karakikes I, Rego S, Cipriano A, Snyder M, et al. iPSC modeling of RBM20-deficient DCM identifies upregulation of RBM20 as a therapeutic strategy. *Cell Rep*. 2020;32:108117. doi: 10.1016/j.celrep.2020.108117
4. Nishiyama T, Zhang Y, Cui M, Li H, Sanchez-Ortiz E, McAnally JR, Tan W, Kim J, Chen K, Xu L, et al. Precise genomic editing of pathogenic mutations in RBM20 rescues dilated cardiomyopathy. *Sci Transl Med*. 2022;14:eade1633. doi: 10.1126/scitranslmed.ade1633
5. Eberl H, Rebs S, Hoppe S, Sedaghat-Hamedani F, Kayvanpour E, Meder B, Streckfuss-Bomeke K. Generation of an RBM20-mutation-associated left-ventricular non-compaction cardiomyopathy iPSC line (UMGi255-A) into a DCM genetic background to investigate monogenetic cardiomyopathies. *Stem Cell Res*. 2024;74:103290. doi: 10.1016/j.scr.2023.103290
6. Kornienko J, Rodriguez-Martinez M, Fenzl K, Hinze F, Schraivogel D, Grosch M, Tunaj B, Lindenhofer D, Schraft L, Kueblbeck M, et al. Mislocalization of pathogenic RBM20 variants in dilated cardiomyopathy is caused by loss-of-interaction with transportin-3. *Nat Commun*. 2023;14:4312. doi: 10.1038/s41467-023-39965-6
7. Gaertner A, Klauke B, Felski E, Kassner A, Brodehl A, Gerdes D, Stanasiuk C, Ebbinghaus H, Schulz U, Dubowy KO, et al. Cardiomyopathy-associated mutations in the RS domain affect nuclear localization of RBM20. *Hum Mutat*. 2020;41:1931–1943. doi: 10.1002/humu.24096
8. Brodehl A, Ebbinghaus H, Gaertner-Rommel A, Stanasiuk C, Klauke B, Milting H. Functional analysis of DES-p.L398P and RBM20-p.R636C. *Genet Med*. 2019;21:1246–1247. doi: 10.1038/s41436-018-0291-2
9. Robyns T, Willems R, Van Cleemput J, Jhangiani S, Muzny D, Gibbs R, Lupski JR, Breckpot J, Devriendt K, Corveleyn A. Whole exome sequencing in a large pedigree with DCM identifies a novel mutation in RBM20. *Acta Cardiol*. 2020;75:748–753. doi: 10.1080/00015385.2019.1674490
10. Beqqali A, Bollen IA, Rasmussen TB, van den Hoogenhof MM, van Deutekom HW, Schafer S, Haas J, Meder B, Sorensen KE, van Oort RJ, et al. A mutation in the glutamate-rich region of RNA-binding motif protein 20 causes dilated cardiomyopathy through missplicing of titin and impaired Frank-Starling mechanism. *Cardiovasc Res*. 2016;112:452–463. doi: 10.1093/cvr/cvw192
11. Yamamoto T, Sano R, Miura A, Imasaka M, Naito Y, Nishiguchi M, Ihara K, Otani N, Kominato Y, Ohmuraya M, et al. I536T variant of RBM20 affects splicing of cardiac structural proteins that are causative for developing dilated cardiomyopathy. *J Mol Med (Berl)*. 2022;100:1741–1754. doi: 10.1007/s00109-022-02262-8
12. Yamamoto T, Miura A, Itoh K, Takeshima Y, Nishio H. RNA sequencing reveals abnormal LDB3 splicing in sudden cardiac death. *Forensic Sci Int*. 2019;302:109906. doi: 10.1016/j.forsciint.2019.109906
13. Floyd BJ, Njoroge JN, Krysov VA, Gomes B, Murtha R, Aribeana C, Cannie D, Smith E, Paldino A, Brown EE, et al. The contribution of RBM20 truncating variants to human cardiomyopathy. *medRxiv*. 2025;2025.07.26.25332081. doi: 10.1101/2025.07.26.25332081
14. Hermida A, Ader F, Jedraszak G, Vogel L, Millat G, Beyls C, Martin N, Vernier A, Charron P, Gandjbakhch E. Prognosis for loss-of-function vs hot-spot variants in RBM20-related cardiomyopathy. *Heart Rhythm*. 2025;22:e1040–e1042. doi: 10.1016/j.hrthm.2025.06.009
15. Schlesinger RP, Castrichini M, Garmany R, Witter T, Ackerman MJ, Giudicessi JR. RBM20 truncating variants predict major ventricular arrhythmia risk independent of structural remodeling. *JACC Clin Electrophysiol*. 2025;S2405–500X(25)00822. doi: 10.1016/j.jacep.2025.10.002
16. Miura A, Yamamoto T, Imasaka M, Sugimoto M, Naito Y, Nishiura H, Nishiguchi M, Funayama K, Yamasu Y, Koyama A, et al. Q373fs variant of RBM20 affects splicing and expression of cardiac-related genes and cardiac function: human sudden death case and mouse experiments. *Hum Mol Genet*. 2025;34:1979–1990. doi: 10.1093/hmg/ddaf157
17. van den Hoogenhof MMG, Beqqali A, Amin AS, van der Made I, Aufiero S, Khan MAF, Schumacher CA, Jansweijer JA, van Spaendonck-Zwarts KY, Remme CA, et al. RBM20 mutations induce an arrhythmogenic dilated cardiomyopathy related to disturbed calcium handling. *Circulation*. 2018;138:1330–1342. doi: 10.1161/CIRCULATIONAHA.117.031947
18. Anzalone AV, Randolph PB, Davis JR, Sousa AA, Koblan LW, Levy JM, Chen PJ, Wilson C, Newby GA, Raguram A, et al. Search-and-replace genome editing without double-strand breaks or donor DNA. *Nature*. 2019;576:149–157. doi: 10.1038/s41586-019-1711-4
19. Ruijter JM, Ramakers C, Hoogaars WM, Karlen Y, Bakker O, van den Hoff MJ, Moorman AF. Amplification efficiency: linking baseline and bias in the analysis of quantitative PCR data. *Nucleic Acids Res*. 2009;37:e45. doi: 10.1093/nar/gkp045
20. Galaxy C. The Galaxy platform for accessible, reproducible, and collaborative data analyses: 2024 update. *Nucleic Acids Res*. 2024;52:W83–W94. doi: 10.1093/nar/gkae410
21. Love MI, Huber W, Anders S. Moderated estimation of fold change and dispersion for RNA-seq data with DESeq2. *Genome Biol*. 2014;15:550. doi: 10.1186/s13059-014-0550-8
22. Wu T, Hu E, Xu S, Chen M, Guo P, Dai Z, Feng T, Zhou L, Tang W, Zhan L, et al. clusterProfiler 4.0: A universal enrichment tool for interpreting omics data. *Innovation (Camb)*. 2021;2:100141. doi: 10.1016/j.xinn.2021.100141
23. Wang Y, Xie Z, Kutschera E, Adams JI, Kadash-Edmondson KE, Xing Y. rMATS-turbo: an efficient and flexible computational tool for alternative splicing analysis of large-scale RNA-seq data. *Nat Protoc*. 2024;19:1083–1104. doi: 10.1038/s41596-023-00944-2
24. Guo W, Schafer S, Greaser ML, Radke MH, Liss M, Govindarajan T, Maatz H, Schulz H, Li S, Parrish AM, et al. RBM20, a gene for hereditary cardiomyopathy, regulates titin splicing. *Nat Med*. 2012;18:766–773. doi: 10.1038/nm.2693
25. Roselli C, Yu M, Nauffal V, Georges A, Yang Q, Love K, Weng LC, Delling FN, Maurya SR, Schrolkamp M, et al. Genome-wide association study reveals novel genetic loci: a new polygenic risk score for mitral valve prolapse. *Eur Heart J*. 2022;43:1668–1680. doi: 10.1093/eurheartj/ehac049
26. Li D, Morales A, Gonzalez-Quintana J, Norton N, Siegfried JD, Hofmeyer M, Hershberger RE. Identification of novel mutations in RBM20 in patients with dilated cardiomyopathy. *Clin Transl Sci*. 2010;3:90–97. doi: 10.1111/j.1752-8062.2010.00198.x
27. Tukker M, Te Rijdt WP, Amin AS, Morris-Rosendahl DJ, Hirsch A, Ben-Haim Y, Houweling AC, Varnava A, Behr ER, Edwards M, et al. High incidence of malignant arrhythmias and heart failure in patients with RBM20-associated cardiomyopathy: a multicenter cohort study and review of the literature. *Int J Cardiol*. 2025;434:133350. doi: 10.1016/j.ijcard.2025.133350
28. Methawasin M, Zhang Y, Gregorich ZR, He Y, Liu C, Muldoon J, Hourani Z, Smith JE 3rd, Granzier H, Guo W. Reducing granules without splicing restoration alleviates RBM20 cardiomyopathy. *Circ Res*. 2025;136:1134–1146. doi: 10.1161/CIRCRESAHA.124.324781
29. Bertero A, Fields PA, Ramani V, Bonora G, Yardimci GG, Reinecke H, Pabon L, Noble WS, Shendure J, Murry CE. Dynamics of

genome reorganization during human cardiogenesis reveal an RBM20-dependent splicing factory. *Nat Commun*. 2019;10:1538. doi: 10.1038/s41467-019-09483-5
30. Upadhyay SK, Mackereth CD. Structural basis of UCUU RNA motif recognition by splicing factor RBM20. *Nucleic Acids Res*. 2020;48:4538–4550. doi: 10.1093/nar/gkaa168
31. Dauksaite V, Gotthardt M. Molecular basis of titin exon exclusion by RBM20 and the novel titin splice regulator PTB4. *Nucleic Acids Res*. 2018;46:5227–5238. doi: 10.1093/nar/gky165
32. Fenix AM, Miyaoka Y, Bertero A, Blue SM, Spindler MJ, Tan KKB, Perez-Bermejo JA, Chan AH, Mayerl SJ, Nguyen TD, et al. Gain-of-function cardiomyopathic mutations in RBM20 rewire splicing regulation and re-distribute ribonucleoprotein granules within processing bodies. *Nat Commun*. 2021;12:6324. doi: 10.1038/s41467-021-26623-y
33. Zhang Y, Gregorich ZR, Wang Y, Braz CU, Zhang J, Liu Y, Liu P, Shen J, Aori N, Hacker TA, et al. Disruption of the nuclear localization signal in RBM20 is causative in dilated cardiomyopathy. *JCI Insight*. 2023;8:e170001. doi: 10.1172/jci.insight.170001